

Constraints on feedback processes during the formation of early-type galaxies

M. Trevisan¹, I. Ferreras², I.G. de La Rosa^{3,4,5}, F. La Barbera⁶, R. R. de Carvalho⁷

⁽¹⁾ *Universidade de São Paulo/IAG, São Paulo, Brazil*

⁽²⁾ *MSSL, University College London, Holmbury St Mary, Dorking, Surrey RH5 6NT, UK*

⁽³⁾ *Instituto de Astrofísica de Canarias (IAC), E-38200 La Laguna, Tenerife, Spain*

⁽⁴⁾ *Department of Physics and Astronomy, University College London, Gower Street, London, WC1E 6BT*

⁽⁵⁾ *Departamento de Astrofísica, Universidad de La Laguna, E-38205 La Laguna, Tenerife, Spain*

⁽⁶⁾ *INAF – Osservatorio Astronomico di Capodimonte, Napoli, Italy*

⁽⁷⁾ *Instituto Nacional de Pesquisas Espaciais/MCT, S. J. dos Campos, Brazil*

trevisan@astro.iag.usp.br

ABSTRACT

Galaxies are found to obey scaling relations between a number of observables. These relations follow different trends at the low- and the high-mass ends. The processes driving the curvature of scaling relations remain uncertain. In this letter, we focus on the specific family of early-type galaxies, deriving the star formation histories of a complete sample of visually classified galaxies from SDSS-DR7 over the redshift range $0.01 < z < 0.025$, covering a stellar mass interval from 10^9 to $3 \times 10^{11} M_{\odot}$. Our sample features the characteristic “knee” in the surface brightness vs. mass distribution at $M_{\star} \sim 3 \times 10^{10} M_{\odot}$. We find a clear difference between the age and metallicity distributions of the stellar populations above and beyond this knee, which suggests a sudden transition from a constant, highly efficient mode of star formation in high-mass galaxies, gradually decreasing towards the low-mass end of the sample. At fixed mass, our early-type sample is more efficient in building up the stellar content at early times in comparison to the general population of galaxies, with half of the stars already in place by redshift $z \sim 2$ for all masses. The metallicity-age trend in low-mass galaxies is not compatible with infall of metal-poor gas, suggesting instead an outflow-driven relation.

Subject headings: Galaxies: formation — Galaxies: evolution — Galaxies: stellar content

1. Introduction

The conversion of gas into stars in galaxies and the role of feedback mechanisms has been one of the key aspects of extragalactic astrophysics over the past decades. Several baryonic processes regulate the star formation efficiency within dark matter haloes. Simulations of galaxy formation and semi-analytical models have shown that it is only within haloes in a mass range around $M_{\text{halo}} \sim M_{\text{shock}} \sim 10^{12} M_{\odot}$ where baryons can form stars efficiently (Cattaneo et al. 2011; Moster et al. 2010; Bouché et al. 2010; Guo et al. 2011). Above this limit, gravitational shock heating and AGN feedback suppress the gas accretion (Dekel & Birnboim 2006; Kereš et al. 2009, 2005; Birnboim & Dekel 2003; Cattaneo et al. 2009, 2011). For galaxies within haloes with masses below $\sim 10^{12} M_{\odot}$, other processes are usually invoked to explain the star formation suppression, for instance, reionization of the IGM (Mamon et al. 2010; Cattaneo et al. 2011). The energy liberated by supernova explosions can eject the gas from haloes with circular velocity $\lesssim 100 \text{ km s}^{-1}$, quenching star formation (Dekel & Silk 1986).

The fraction of mass acquired via mergers is also a function of stellar mass. For example, the semi-analytical models of De Lucia et al. (2006) show that the number of effective progenitors of galaxies with stellar masses $\lesssim 10^{11} M_{\odot}$ is less than two, while this number can be as large as five for galaxies with $M_{\star} \sim 10^{12} M_{\odot}$. According to Cattaneo et al. (2011), the dependence of feedback and merger processes on stellar mass defines three galaxy formation regimes. Stellar mass $\sim 10^{11} M_{\odot}$ marks the transition between two dominant mechanisms: gas accretion ($M_{\star} \lesssim 10^{11} M_{\odot}$) and gas-poor mergers ($M_{\star} \gtrsim 10^{11} M_{\odot}$). A third regime, set immediately below $\sim 10^{11} M_{\odot}$, is characterized by the increasing contribution of a population built by gas-rich mergers. The contribution of these mass-dependent processes explain the well known dichotomy among early-type galaxies (e.g. Kang et al. 2007), supported by many observations, like e.g. a characteristic mass scale (Kauffmann et al. 2003), and a well-defined mass-metallicity relation (see e.g. Tremonti et al. 2004).

If the dichotomy originates from the mass-dependent role played by feedback, gas accretion, gas-rich and gas-poor mergers, we would expect to find signatures of these processes on the formation history of galaxies with respect to stellar mass. In this letter, the star formation history of a sample of galaxies over a wide range of stellar mass (from 10^9 to $10^{11.5} M_{\odot}$) has been examined for the presence of those signatures.

This letter is organized as follows: in Sect. 2, we describe the sample; in Sect. 3, we present a detailed study of the stellar populations using a spectral fitting code, which also is able to return the star formation history. Finally, we summarize and discuss our results in Sect. 4. Throughout the paper, we adopt a cosmology with $H_0 = 70 \text{ km s}^{-1} \text{ Mpc}^{-1}$, $\Omega_{\text{m}} = 0.3$ and $\Omega_{\Lambda} = 0.7$.

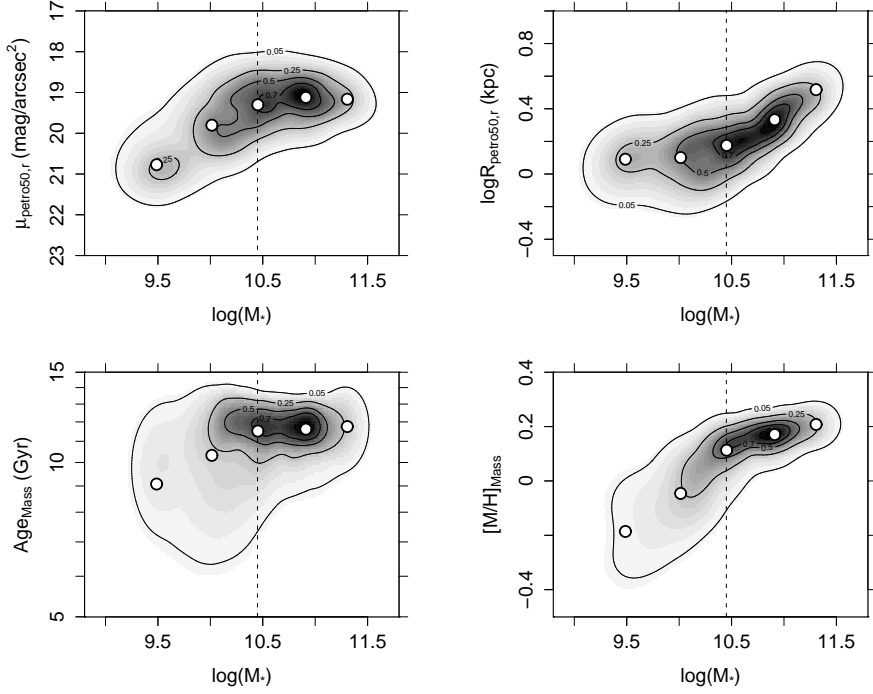


Fig. 1.— **Upper panels:** Scaling relations between stellar mass and surface brightness (left) or half-light radius (right). Both quantities are measured with respect to the Petrosian radius measured in the r band. **Bottom panels:** Mass-weighted average age (left) and metallicity (right), as obtained by the STARLIGHT spectral fitting code (see text for details). The grayscale corresponds to the density of points in each graph, with contour lines given at the 90, 70, 50, 25 and 5% levels with respect to the maximum value. The vertical dashed lines indicate $M_* \sim 3 \times 10^{10} M_\odot$, which corresponds to the stellar mass of objects with $\mathcal{M}_{\text{petro},r} = -20.2$, i.e. at the knee in the scaling relations. Median values obtained within mass bins (see Table 1) are shown in each panel as open dots.

2. Sample description

Our sample of early-type galaxies was retrieved from SDSS-DR7 (Abazajian et al. 2009), selecting galaxies in the redshift range between 0.01 and 0.025, brighter than $m_{\text{petro},r} < 17.77$, where $m_{\text{petro},r}$ is the Petrosian magnitude in the r-band. This limit roughly corresponds to the magnitude at which the SDSS spectroscopy is complete (Strauss et al. 2002). The redshift limits chosen provide a 95% complete sample between $\mathcal{M}_{\text{petro},r} \sim -20$ and ~ -17.46 , where $\mathcal{M}_{\text{petro},r}$ is the k-corrected SDSS Petrosian absolute magnitude in r-band, obtained with the `kcorrect` code (version 4.2) of Blanton et al. (2003), choosing as reference the median redshift of the sample ($z_0=0.021$). See La Barbera et al. (2008) for details on the estimation of the completeness limits.

To select objects from the SDSS database, we define a flag mask, excluding those objects which are: *i*) blended, i. e., with more than one photometric peak¹; *ii*) too bright (detections of $> 200 \sigma$); *iii*) too large ($r > 4'$ or a deblend with $r > 1/2$ frame); *iv*) saturated; *v*) located close to the edge of a frame or *vi*) in a region where the sky measurement failed, thus the photometry is compromised; objects which *vii*) are part of the extended wing of a bright star or *viii*) which may be an electronic ghost of a bright star were also excluded. In addition, only objects with no spectroscopic warning on (i.e. `zWarning` attribute set to zero) were selected. This selection returns 10187 objects.

Early-type galaxies obey well-studied scaling relations. Several morphological classification indicators have been proposed from the parameters of the SDSS pipeline (e.g. Strateva et al. 2001). However, it is still unclear whether these indicators can be applied to low mass systems. Previous work has shown that dwarf elliptical galaxies do not have the same surface brightness profile as their giant counterparts (Graham & Guzmán 2003), or similar star formation histories (Koleva et al. 2009), even featuring weak spiral structures (Lisker 2009). Hence, we cannot use the standard SDSS attributes such as `eClass` or `fracDev`. Instead, visual inspection is the most reliable indicator of an early-type morphology. We use the classification from the Galaxy Zoo project (Lintott et al. 2011), selecting only galaxies classified as elliptical. We found 10138 (99.7%) galaxies from our sample in the Galaxy Zoo database. Among them, 1359 are classified as ellipticals (spirals and unreliable classifications are discarded). The completeness constraint – in $\mathcal{M}_{\text{petro},r}$ – results in a final sample of 1328 objects. A further visual inspection was carried out by the authors to confirm the morphological classification.

3. Stellar content

Age, metallicity, stellar mass and velocity dispersion were derived using the spectral fitting code `STARLIGHT` (Cid Fernandes et al. 2005). Before running the code, the observed spectra are corrected for foreground extinction and de-redshifted, and the models are degraded to match the

¹Since we are using objects from the primary catalog, this selection is equivalent to exclude objects with two or more peaks, which were not deblended

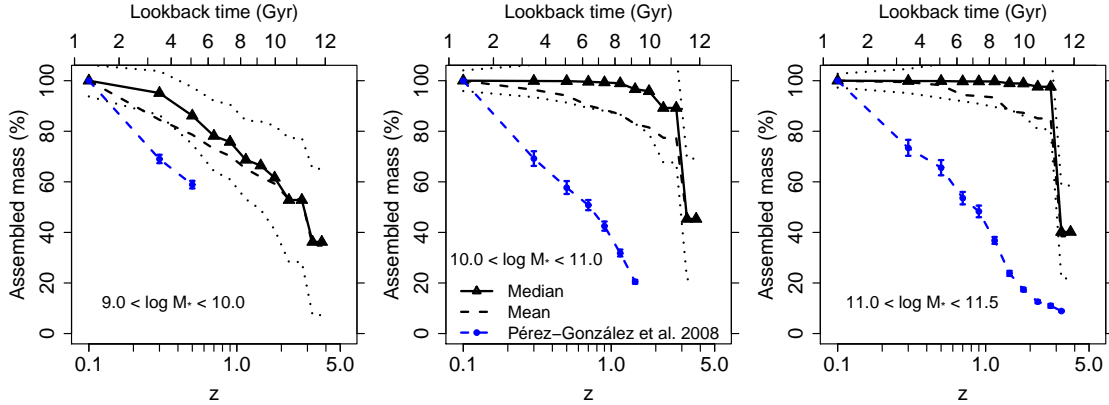


Fig. 2.— Fraction of assembled stellar mass as a function of redshift. The panels show the fraction of mass normalized by the mass of galaxies at $z \sim 0.1$. Black triangles and solid (dashed) lines show median (mean) values for the present sample of early-type galaxies, with 1σ confidence intervals being marked as dotted lines. Results by Pérez-González et al. (2008) are plotted as (blue) solid circles with error bars, and dashed blue curves.

wavelength-dependent resolution of the spectrum of each galaxy, as described in La Barbera et al. (2010b).

We used SSP models based on the Medium resolution INT Library of Empirical Spectra (MILES, Sánchez-Blázquez et al. 2006), using the code presented in Vazdekis et al. (2010), using version 9.1 (Falcón-Barroso et al. 2011). They have a spectral resolution of $\sim 2.5 \text{ \AA}$, almost constant with wavelength. A basis grid of 162 SSPs was selected, covering ages in the range of $0.07 - 12.6 \text{ Gyr}$, and with $[M/H] = \{-1.71, -1.31, -0.71, -0.38, 0.00, +0.20\}$. The models use a Kroupa (2001) Universal IMF with slope = 1.30, and isochrones by Girardi et al. (2000). The stellar masses – computed within the fiber aperture – are extended to the full extent of the galaxy by computing the difference between fiber and model magnitudes in the z band. The stellar mass is then $\log(M_\star) = \log(M_\star)' + 0.4 (m_{\text{fiber},z} - m_{\text{model},z})$.

We compare the results from STARLIGHT with different set-up parameters and different grids. We find no systematic trends, with differences typically within $\pm 20\%$. A detailed study of how results are affected by changes on the set-up parameters of STARLIGHT and different SSP model assumptions will be given in a forthcoming paper (Trevisan et al., in prep.). Variations in the SSP optical colors due to different IMF shapes are very small (see e.g. Vazdekis et al. 2010). Since STARLIGHT uses all the spectral information available, different IMFs are not expected to affect our results. Hence, if a systematic change of the IMF is present (as suggested by, e.g. van Dokkum & Conroy 2011) from low- to high-mass early-type galaxies, the net result would be a change of the stellar mass that corresponds to the position of the knee, keeping the derived stellar population properties presented here unchanged.

4. Results and discussion

In this letter, we study the star formation histories of a sample of ~ 1300 visually-selected elliptical galaxies by means of a spectral fitting method. For each galaxy we determine the stellar mass, metallicity, age and star formation history (SFH). Fig. 1 shows both the photometric scaling relations (upper panels), along with the scaling of the derived average ages and metallicities, weighted in mass (bottom panels). The plots of surface brightness μ_{Petro} and Petrosian radius *vs.* stellar mass provide similar information, considering that μ_{Petro} is derived from Petrosian radius and luminosity, with the latter following the stellar mass of a galaxy. We bin the sample into five subsamples in stellar mass, indicated by blue dots in Fig. 1. Table 1 presents the median properties of the stellar populations for each bin. Regarding the age and metallicity scaling relation (bottom panels in Fig. 1), a clear change in the slope of $[\text{M}/\text{H}]$ *vs.* stellar mass is apparent at $\sim 3 \times 10^{10} M_{\odot}$, equivalent to an absolute magnitude of $\mathcal{M}_{\text{dev},r} \sim -20.2$, below which the metallicity decreases linearly with mass. This corresponds approximately to the position of the knee seen in the photometric scale relations. The age distribution is more complex, with a homogeneous population of old galaxies for $M_{\star} \gtrsim 10^{10} M_{\odot}$, and an increased scatter towards younger ages with decreasing mass.

It is not clear whether the dichotomy in structural properties has the same origin as the stellar population properties (see e.g. Graham & Guzmán 2003; Janz & Lisker 2008; Côté et al. 2008). The fact that the knee in the photometric scaling relations has a counterpart in the stellar population properties might indicate the processes regulating the star formation also affect the structural properties of galaxies. For example, feedback mechanisms might affect galaxy sizes, since the gas is pushed out of galaxies by outflows and might be converted into stars at large radii. (e.g. Fan et al. 2008, 2010; Damjanov et al. 2009).

4.1. Star formation history

Besides the averaged age and metallicity, spectral fitting provides a wealth of additional information on the star formation histories of individual galaxies. For a given spectrum, a STARLIGHT run returns the contribution, as a percentage of mass, from each *basis* SSP. This distribution traces directly the star formation history. For each galaxy in the sample, we determine the “cumulative” mass fraction, i.e. the fraction of stars older than a given age, as a function of age. Then, we average the cumulative distributions over all galaxies within each mass bin. The age of the distribution at the 50th and 80th percentiles in stellar mass is presented in Table 1. Galaxies with mass $\gtrsim 10^{10} M_{\odot}$ form their stars early and over a very short period of time, with 80% of their stars being older than ~ 11 Gyr. Galaxies in the low mass bins also have a very old stellar population. However, the time required to form 80% of the stellar mass is $\sim 5 - 6$ Gyr longer than that required by more massive galaxies. Hence, in early-type galaxies, *downsizing* should be interpreted as a more extended period of formation in low mass galaxies (instead of an overall later process of formation).

We compare our results with Pérez-González et al. (2008). Their study is based on a sample

of ~ 28000 objects of all morphological types at $0 < z < 4$ to constrain the evolution of the stellar mass content in galaxies as a function of redshift. We rebin our sample into three subsamples with masses ranging from $\log(M_\star) = 9.0 - 10.0$, $10.0 - 11.0$, and $11.0 - 11.5$, which correspond to the first three bins of Pérez-González et al. (2008). Figure 2 shows the cumulative mass fractions as a function of redshift. In all three bins, early-type galaxies are formed in a much more efficient process, in contrast to the sample of Pérez-González et al. (2008), although the difference is more pronounced in the most massive bin. The large difference is due to the fact that their sample includes galaxies of all morphological types. In contrast, the analysis of the stellar populations of visually classified early-type galaxies at $z \lesssim 1$, yield a short-lived and early process of star formation (Ferreras et al. 2009b), consistent with our findings. Furthermore, the present sample is susceptible to aperture effects, since all galaxies are observed through a fiber with fixed angular diameter. Table 1 reports the mean aperture for each mass bin. The aperture A is defined as the ratio between the radius of the SDSS fiber and the half-light Petrosian radius measured in the r band, $A = R_{\text{fiber}}/R_{\text{petro50},r}$. The mean aperture varies from $A \sim 0.5$ in the first two bins to ~ 0.2 in the more massive bin. Assuming that the internal metallicity gradient of early-type galaxies varies from about -0.4 kpc^{-1} at high mass (La Barbera et al. 2011) to negligible at lowest mass (e.g. Koleva et al. 2011), the above variation of A would imply a change of ~ 0.16 in $[M/H]$, i.e. smaller than that of ~ 0.4 seen for the range of masses in Table 1. In addition, the typical internal scatter of stellar population properties is larger than systematics due to aperture effects. Since age gradients are generally small in (massive) ETGs, aperture effects are also likely not to drive the variation of galaxy age with stellar mass. This conclusion is further supported by our analysis of the waveband dependence of the Fundamental Plane relation of bright ETGs (La Barbera et al. 2010a), as we found that total (i.e. within an infinite aperture) metallicity and age do actually increase with stellar mass.

Table 1: Stellar population properties as a function of stellar mass.

$\log(M_\star)$ interval	9.2 – 9.7	9.7 – 10.2	10.2 – 10.7	10.7 – 11.2	11.2 – 11.7
Number of objects	156	293	410	360	84
L-weighted Age (Gyr)	6.5 ± 3.6	8.8 ± 3.3	10.3 ± 2.3	10.2 ± 1.6	9.8 ± 1.2
M-weighted Age (Gyr)	9.1 ± 2.8	10.3 ± 2.4	11.5 ± 1.8	11.6 ± 1.4	11.8 ± 1.2
50% of stars older than (Gyr)	11.2	12.4	12.4	12.4	12.4
80% of stars older than (Gyr)	5.3	8.2	11.5	11.6	11.7
L-weighted $[M/H]$	-0.3 ± 0.2	-0.2 ± 0.2	0.0 ± 0.1	0.1 ± 0.1	0.1 ± 0.1
M-weighted $[M/H]$	-0.2 ± 0.2	-0.1 ± 0.1	0.1 ± 0.1	0.2 ± 0.1	0.2 ± 0.1
$R_{\text{fiber}}/R_{\text{petro50},r}$	0.51 ± 0.19	0.50 ± 0.19	0.42 ± 0.15	0.30 ± 0.09	0.21 ± 0.05

4.2. Constraints of feedback processes

These results indicate that the processes regulating star formation in the low- and high-mass regimes leave different signatures on the SFH. Tab. 1 shows that galaxies within the three more massive bins have similar ages and metallicities, with 80% of their stellar mass formed at approximately the same redshift. The ages and metallicities are almost constant from the third to the fifth mass bins. On the other hand, the low mass bins show a gradual decrease of age and metallicity with decreasing stellar mass. Galaxies in all bins have roughly half of their stars formed before redshift $z \sim 2 - 3$. For the most massive galaxies, the additional 30% of the stars is formed within ~ 1 Gyr. Hence, the star formation in these galaxies after a redshift $z \sim 1$ can be considered “residual”. On the other hand, galaxies with mass ranging from $\log(M_*) = 9.2$ to 9.7 have 80% of their star formed only at $z \sim 0.5$. Our results indicate that massive objects form faster and low mass systems have a more extended star formation history than suggested by models (e.g. De Lucia et al. 2006).

The feedback mechanism commonly invoked to explain the regulation of star formation in low mass systems is supernovae-driven winds (e.g. Larson 1974; Ferrara & Tolstoy 2000; Kereš et al. 2009). The chemical enrichment of low-mass galaxies indicate that the process regulating the star formation in these galaxies should be strong enough to eject metals out of the galaxy. However, it is not able to quench the star formation completely. Alternatively, these systems may be continuously being fuelled by infalling IGM gas at low metallicity.

Figure 3 shows the mass-weighted $[M/H]$ as a function of stellar population age. The metal enrichment is shown down to the age when approximately 80% of the stellar mass is formed². Galaxies in the three most massive bins form their stars very quickly, and 80% of their stars are older than 11 Gyr. For this reason, only two points are shown for these three bins. The figure shows a consistent trend of chemical enrichment, whereby the younger populations are more metal rich, a result that supports the idea that the mass-metallicity trend cannot be explained by the infall of metal-poor gas, requiring instead a feedback mechanism that preferentially removes metals from low-mass galaxies. Supernova feedback can account for these “metal-enhanced outflows”. Since metals are formed in SN events, SN-driven winds are metal-enhanced with respect to the star-forming gas. Most of the metals mixed with the hot gas are able to leave the galaxy, whereas only a small fraction of cool ISM gas is lost (see e.g. Tremonti et al. 2004; Mac Low & Ferrara 1999; Ferrara & Tolstoy 2000). This scenario is compatible with the $[M/H]$ *vs.* stellar mass relation shown in Fig. 1. SN-driven feedback is expected to be dominant in low-mass systems, whereas feedback processes in massive galaxies leave a sharp truncation in the SFH, giving rise to different slopes above and below the characteristic mass. The position of the knee in the photometric scaling relations suggests that the interplay of these feedback mechanisms leaves an imprint on galaxy sizes and surface brightness. Aperture effect is not expected to affect these results, as galaxies in a given

²Notice that, for a given mass bin, the lowest Age in Fig. 3 does not correspond exactly to the value of $t_{80\%}$ in Tab. 1, because of the discreteness of SSP ages in the STARLIGHT input basis (see Sect. 3).

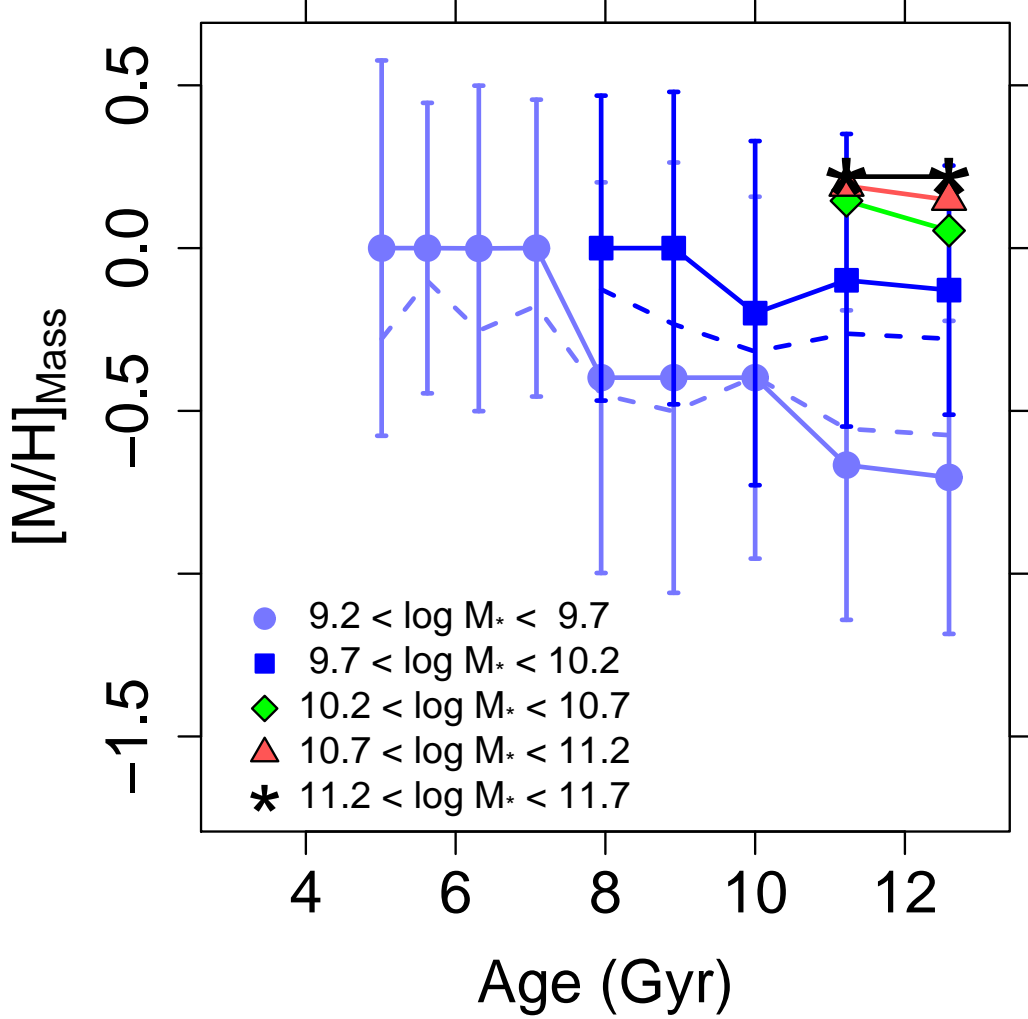


Fig. 3.— Mass-weighted metallicity as a function of stellar population age, in bins of stellar mass. The metal enrichment is shown until 80% of the mass is assembled. For this reason, only two points at 11.2 and 12.6 Gyr are shown for the three most massive bins. This corresponds to the age of the two oldest SSPs used in the spectral fitting. The solid (dashed) lines indicate the median (mean) values. Error bars reflect mainly the discreteness of the SSP model grid; the metallicities available in the grid are spaced by ~ 0.4 .

mass range have similar $r_{\text{fiber}}/r_{\text{petro}}$ ratios. In addition, we verified that the trend is not driven by the age-metallicity degeneracy. We ran STARLIGHT on simulated spectra with no chemical-

enrichment and similar S/N and star-formation history as galaxies at lowest-mass, and we do not find any significant correlation between $[M/H]_{\text{Mass}}$ and Age.

The SFH of high-mass galaxies indicate that their stars were already formed before $z \sim 2$. Several studies have shown that high mass systems are assembled mainly via mergers (De Lucia et al. 2006; Cattaneo et al. 2011). However, our results constrain the main epoch of growth via mergers to $z \gtrsim 2$, unless the mergers proceed mainly via gas poor progenitors. Alternatively, these systems can be already in place at high redshift, as suggested by the weaker number density evolution with redshift for the most massive galaxies between $z \sim 1.5$ and 0. (see e.g. Conselice et al. 2007; Ferreras et al. 2009a; Banerji et al. 2010). The cold mode of galaxy formation (Kereš et al. 2005; Guo et al. 2011; Dekel et al. 2009b,a) can account for the required high star formation efficiency at high redshift. However, it is still not clear how this process can result in the spheroidal morphologies we see in place at $z \sim 1$.

We thank the referee for very constructive comments that led to improvements in our manuscript. MT acknowledges a FAPESP fellowship no. 2008/50198-3. IGR acknowledges a grant from the Spanish Secretaria General de Universidades, in the frame of its programme to promote mobility of Spanish researchers to foreign centers. A full acknowledgement regarding the use of the Sloan Digital Sky Survey can be found in this website: <http://www.sdss.org/collaboration/credits.html>

REFERENCES

- Abazajian, K. N., Adelman-McCarthy, J. K., Agüeros, M. A., et al. 2009, *ApJS*, 182, 543
- Banerji, M., Ferreras, I., Abdalla, F. B., Hewett, P., & Lahav, O. 2010, *MNRAS*, 402, 2264
- Birnboim, Y., & Dekel, A. 2003, *MNRAS*, 345, 349
- Blanton, M. R., Brinkmann, J., Csabai, I., et al. 2003, *AJ*, 125, 2348
- Bouché, N., Dekel, A., Genzel, R., et al. 2010, *ApJ*, 718, 1001
- Cattaneo, A., Mamon, G. A., Warnick, K., & Knebe, A. 2011, *A&A*, 533, A5
- Cattaneo, A., Faber, S. M., Binney, J., et al. 2009, *Nature*, 460, 213
- Cid Fernandes, R., Mateus, A., Sodré, L., Stasińska, G., & Gomes, J. M. 2005, *MNRAS*, 358, 363
- Conselice, C. J., Bundy, K., Trujillo, I., et al. 2007, *MNRAS*, 381, 962
- Côté, P., Ferrarese, L., Jordán, A., et al. 2008, in *IAU Symposium*, Vol. 245, *IAU Symposium*, ed. M. Bureau, E. Athanassoula, & B. Barbuy, 395–398
- Damjanov, I., McCarthy, P. J., Abraham, R. G., et al. 2009, *ApJ*, 695, 101

- De Lucia, G., Springel, V., White, S. D. M., Croton, D., & Kauffmann, G. 2006, *MNRAS*, 366, 499
- Dekel, A., & Birnboim, Y. 2006, *MNRAS*, 368, 2
- Dekel, A., Sari, R., & Ceverino, D. 2009a, *ApJ*, 703, 785
- Dekel, A., & Silk, J. 1986, *ApJ*, 303, 39
- Dekel, A., Birnboim, Y., Engel, G., et al. 2009b, *Nature*, 457, 451
- Falcón-Barroso, J., Sánchez-Blázquez, P., Vazdekis, A., et al. 2011, *A&A*, 532, A95
- Fan, L., Lapi, A., Bressan, A., et al. 2010, *ApJ*, 718, 1460
- Fan, L., Lapi, A., De Zotti, G., & Danese, L. 2008, *ApJL*, 689, L101
- Ferrara, A., & Tolstoy, E. 2000, *MNRAS*, 313, 291
- Ferreras, I., Lisker, T., Pasquali, A., & Kaviraj, S. 2009a, *MNRAS*, 395, 554
- Ferreras, I., Pasquali, A., Malhotra, S., et al. 2009b, *ApJ*, 706, 158
- Girardi, L., Bressan, A., Bertelli, G., & Chiosi, C. 2000, *A&AS*, 141, 371
- Graham, A. W., & Guzmán, R. 2003, *AJ*, 125, 2936
- Guo, Q., White, S., Boylan-Kolchin, M., et al. 2011, *MNRAS*, 413, 101
- Janz, J., & Lisker, T. 2008, *ApJL*, 689, L25
- Kang, X., van den Bosch, F. C., & Pasquali, A. 2007, *MNRAS*, 381, 389
- Kauffmann, G., Heckman, T. M., White, S. D. M., et al. 2003, *MNRAS*, 341, 54
- Kereš, D., Katz, N., Davé, R., Fardal, M., & Weinberg, D. H. 2009, *MNRAS*, 396, 2332
- Kereš, D., Katz, N., Weinberg, D. H., & Davé, R. 2005, *MNRAS*, 363, 2
- Koleva, M., de Rijcke, S., Prugniel, P., Zeilinger, W. W., & Michielsen, D. 2009, *MNRAS*, 396, 2133
- Koleva, M., Prugniel, P., de Rijcke, S., & Zeilinger, W. W. 2011, *MNRAS*, 417, 1643
- Kroupa, P. 2001, *MNRAS*, 322, 231
- La Barbera, F., de Carvalho, R. R., de La Rosa, I. G., & Lopes, P. A. A. 2010a, *MNRAS*, 408, 1335
- La Barbera, F., de Carvalho, R. R., de La Rosa, I. G., et al. 2010b, *MNRAS*, 408, 1313

- La Barbera, F., de Carvalho, R. R., Kohl-Moreira, J. L., et al. 2008, *Publications of the Astronomical Society of the Pacific*, 120, 681
- La Barbera, F., Ferreras, I., de Carvalho, R. R., et al. 2011, *ApJL*, 740, L41
- Larson, R. B. 1974, *MNRAS*, 169, 229
- Lintott, C., Schawinski, K., Bamford, S., et al. 2011, *MNRAS*, 410, 166
- Lisker, T. 2009, *Astronomische Nachrichten*, 330, 1043
- Mac Low, M.-M., & Ferrara, A. 1999, *ApJ*, 513, 142
- Mamon, G. A., Tweed, D., Cattaneo, A., & Thuan, T. X. 2010, *ArXiv e-prints*
- Moster, B. P., Somerville, R. S., Maulbetsch, C., et al. 2010, *ApJ*, 710, 903
- Pérez-González, P. G., Rieke, G. H., Villar, V., et al. 2008, *ApJ*, 675, 234
- Sánchez-Blázquez, P., Peletier, R. F., Jiménez-Vicente, J., et al. 2006, *MNRAS*, 371, 703
- Strateva, I., Ž. Ivezić, Knapp, G. R., et al. 2001, *AJ*, 122, 1861
- Strauss, M. A., Weinberg, D. H., Lupton, R. H., et al. 2002, *AJ*, 124, 1810
- Tremonti, C. A., Heckman, T. M., Kauffmann, G., et al. 2004, *ApJ*, 613, 898
- van Dokkum, P. G., & Conroy, C. 2011, *ApJL*, 735, L13
- Vazdekis, A., Sánchez-Blázquez, P., Falcón-Barroso, J., et al. 2010, *MNRAS*, 404, 1639